

Chapter 2

Principle Techniques of E989

As referenced in Equation 1.2, a particle in a magnetic field will experience a torque which attempts to line up the magnetic dipole moment of the particle with the external field. Because of this, in a dipole field a particles spin will turn at the precession frequency [31]

$$\vec{\omega}_s = -g \frac{q}{2m} \vec{B} - (1 - \gamma) \frac{q}{\gamma m} \vec{B}, \quad (2.1)$$

where as before m is the particles mass, $q = \pm e$ where e is the positive elementary charge, g is the g-factor, γ is the Lorentz relativistic factor, and B is an external magnetic field. The first term is the usual Larmor frequency and the second term is a relativistic correction to the precession frequency called Thomas precession [31].

Similarly, a particle with some momentum will orbit at the cyclotron frequency

$$\vec{\omega}_c = -\frac{q}{\gamma m} \vec{B}. \quad (2.2)$$

By taking the difference between these two frequencies we arrive at the “spin difference frequency”

$$\vec{\omega}_a = \vec{\omega}_s - \vec{\omega}_c = -\frac{g - 2}{2} \frac{q}{m} \vec{B} = -a \frac{q}{m} \vec{B}, \quad (2.3)$$

a frequency that is directly proportional to anomaly a . If $g = 2$ as in a Dirac theory, then the particles spin would turn at the same rate as the momentum vector, and

this spin difference frequency ω_a would be identically zero. If this spin difference frequency for a muon and the external magnetic dipole field can be measured, then the anomalous magnetic moment of the muon a_μ can be measured.

As will be detailed below in Section 2.2, the measurement of the magnetic field is related to the Larmor precession frequency of free protons in water

$$\omega_p = -g_p \frac{e}{2m_p} B, \quad (2.4)$$

where g_p and m_p are the g-factor and mass of the proton respectively. Replacing B and solving for a_μ , we arrive at

$$a_\mu = \frac{g_p}{2} \frac{\omega_a}{\omega_p} \frac{m_\mu}{m_p}. \quad (2.5)$$

Using the magnetic moment formulas for the proton, electron, and muon as shown in Equation 1.1, Equation 2.5 can be transformed to either of the following consistent equations:

$$\begin{aligned} a_\mu &= \frac{g_e}{2} \frac{\omega_a}{\omega_p} \frac{m_\mu}{m_e} \frac{\mu_p}{\mu_e} \\ a_\mu &= \frac{\omega_a/\omega_p}{\lambda - \omega_a/\omega_p} \end{aligned} \quad (2.6)$$

Here the p , e , and μ subscripts stand for the relevant quantities for the proton, electron, and muon respectively. In the second equation $\lambda = \mu_\mu/\mu_p$. As mentioned before the electron g-factor g_e has been measured to extremely high precision, 0.26 ppt [28, 29]. The muon-electron mass ratio m_μ/m_e and muon-proton magnetic moment ratio λ have been measured to 22 ppb [29, 32]. Finally the proton-electron magnetic moment ratio μ_p/μ_e has been measured to 3 ppb [29]. The errors on these terms are small compared to the target uncertainty for E989 of 140 ppb, the measurement of which now comes down to measuring the ratio ω_a/ω_p .

2.1 Measuring ω_a

How can ω_a for muons be measured? The answer lies with two key points in the dynamics of muon decay. Positive muons decay to a positron and two neutrinos, as shown in Figure 2-1a. The first point is that because of the parity violating nature of the weak interaction, the decay positron will be preferentially emitted right-handed, with its spin directed in the same direction as its momentum [33]. The second key point is that angular momentum must be conserved. Consider the most extreme examples of maximum and minimum energy positrons as shown in Figure 2-2. In the muon rest frame, decay positrons with maximum energy will be emitted opposite to the two neutrinos. Since neutrinos and anti-neutrinos must be left and right-handed respectively, thus having their spins anti-parallel and parallel to their momentum, by the law of conservation of angular momentum the positron must have its spin be parallel to the spin of the muon at the time of the decay. By the opposite argument, decay positrons emitted with minimum energy such that the neutrinos are ejected opposite to one another must have their spins be anti-parallel to that of the muon at the time of decay. These two points combined together means that higher energy decay positrons will preferentially be emitted in directions parallel to the muon spin at the time of decay, while lower energy decay positrons will preferentially be emitted in directions anti-parallel to the muon spin at the time of the decay.

This correlation between the emitted direction of the decay positron and the spin of the muon is the signature needed to measure ω_a . By placing an ensemble of polarized muons within a magnetic storage ring, those muons will orbit at the cyclotron frequency and their spins will precess at the Larmor frequency. As they go around the ring they will decay to positrons whose energy and decay directions contain information about the spin of the muon. The differential decay distribution

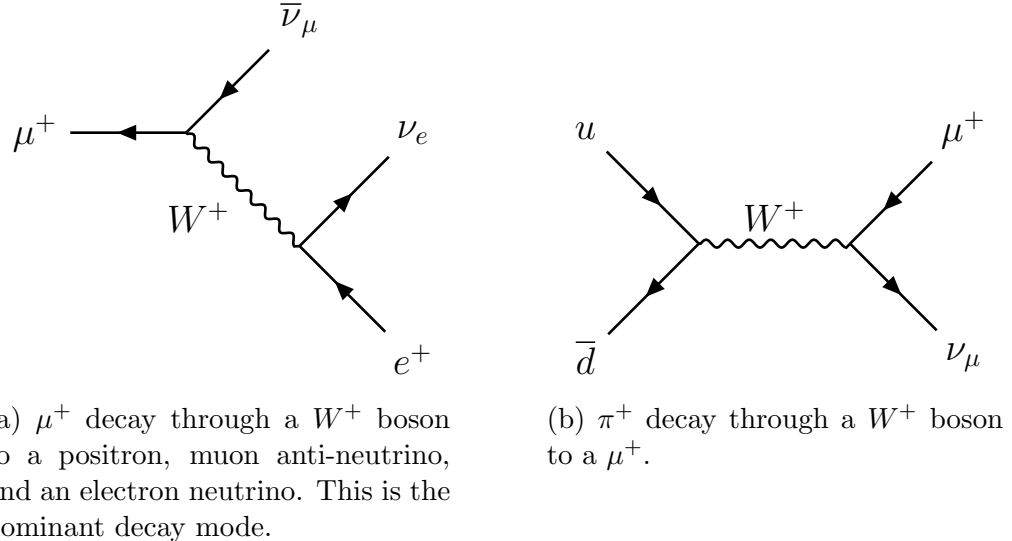


Figure 2·1: Feynman diagrams for muon (left) and pion (right) decay.

Muon decay in the rest frame

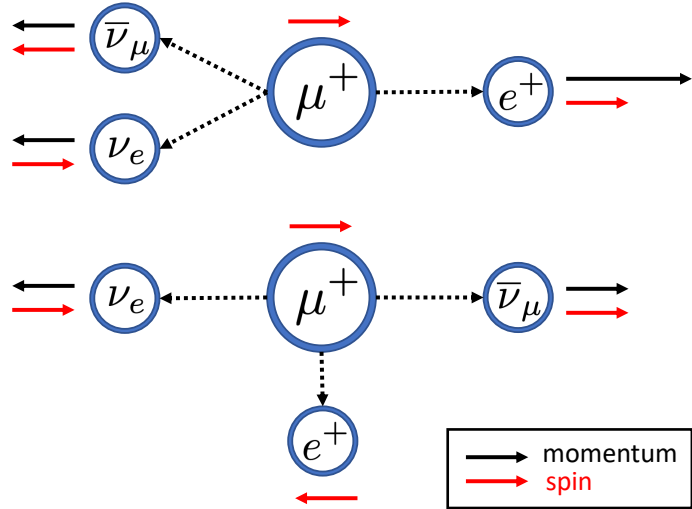


Figure 2·2: Muon decay pictures for maximum and minimum energy decay positrons. Due to the conservation of angular momentum and the single possible helicity states of the decay neutrinos, the spin of the decay positron is exactly parallel to the spin of the muon at the time of the decay for maximum energy decay positrons (top), or anti-parallel for minimum energy decay positrons (bottom).

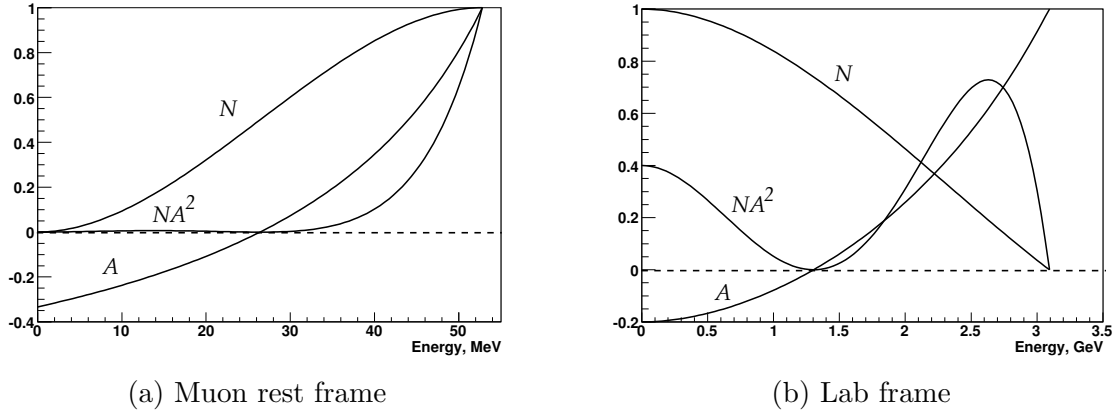


Figure 2·3: Decay number distribution N and asymmetry A in the muon rest frame (left) and in the lab frame (right) as a function of positron energy with a maximum positron energy of 3.1 GeV.

in the muon rest frame is described by [33]

$$dP(y, \theta) \propto N(y)[1 \pm A(y)\cos(\theta)]dyd\Omega, \quad (2.7)$$

where $y = E/E_{max}$ is the energy fraction of the positron, θ is the angle between the spin of the muon and the momentum of the positron $\cos^{-1}(\hat{p} \cdot \hat{s})$, and the \pm stands for the positive and negative muon respectively. $N(y)$ is the number distribution of decay positrons and $A(y)$ is the so called 'asymmetry' encoding the preferred positron decay direction. Here the energy of the positron is assumed to be much greater than its mass. The number distribution and asymmetry are given by [33]

$$N(y) = 2y^2(3 - 2y^2), \quad (2.8)$$

$$A(y) = \frac{2y-1}{3-2y}, \quad (2.9)$$

and are shown in Figure 2.3a.

In the lab frame for high energy positrons, nearly all positrons will be emitted parallel to the muon momentum, which makes it challenging to select purely on the decay angle of the positron. That's not a problem though, as we already know that

That is not

decay positrons with higher energies will be emitted in directions parallel to the muon spin at the time of decay. Essentially, the energy distribution of detected positrons for high energies is modulated by ω_a , or $\theta = \omega_a t + \phi$. The number of detected positrons at some time and energy in the lab frame for some initial number N_0 of muons can then be described by

$$N_d(t, E) = N_0(E) \cdot e^{-t/\gamma\tau_\mu} \cdot [1 + A(E) \cos(\omega_a t + \phi(E))], \quad (2.10)$$

where the d subscript stands for 'detected,' the muons are decaying at a lifetime of $\gamma\tau_\mu$, and all the relevant parameters are energy dependent. Here $N_0(E)$ and $A(E)$ have been transformed from Equations 2.8 and 2.9 to the lab frame,

$$N_0(E) \propto (y - 1)(4y^2 - 5y - 5), \quad (2.11)$$

$$A(E) = \frac{-8y^2 + y + 1}{4y^2 - 5y - 5}, \quad (2.12)$$

where as a reminder $y = E/E_{max}$. Here the polarization of the muons is assumed to be unity. These are shown in Figure 2.3b. To increase the amount of statistics, all positrons above some energy threshold cut E_{th} can be taken as the observable,

$$N_d(t, E_{th}) = N_0(E_{th}) \cdot e^{-t/\gamma\tau_\mu} \cdot [1 + A(E_{th}) \cos(\omega_a t + \phi(E_{th}))], \quad (2.13)$$

where the number and asymmetry of the detected positrons is now calculated by simply integrating Equations 2.11 and 2.12 from y_{th} to 1,

$$N_0(E_{th}) \propto (y_{th} - 1)^2(-y_{th}^2 + y_{th} + 3), \quad (2.14)$$

$$A(E_{th}) = \frac{y_{th}(2y_{th} + 1)}{-y_{th}^2 + y_{th} + 3}, \quad (2.15)$$

where $y_{th} = E_{th}/E_{max}$. By fitting Equation 2.13, ω_a can be extracted. An sample of data adhering to Equation 2.13 is shown in Figure 2.4.

is there a better way?

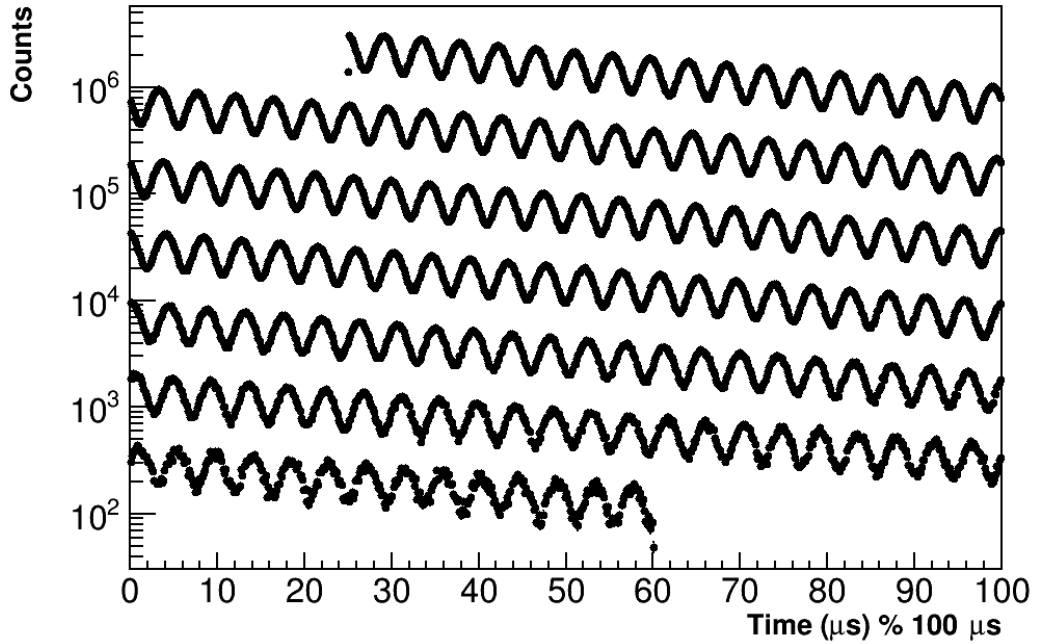


Figure 2.4: The number of detected positrons above some energy threshold ($y \sim 0.55$) as a function of time. The time axis is wrapped around every 100 μs .

2.2 Measuring the magnetic field

In order to measure the magnetic moment of the muon to 140 ppb, the field needs to be both highly uniform, and measured to extreme precision. The E989 goal for the field measurement is 70 ppb. As shown in Equation 2.6 the measurement of the magnetic field has equal weight to that of the precession frequency. A cross-section of the magnetic ring is shown in Figure 2.5. The muons live within a 9 cm² diameter cylindrical storage region at the center of the magnetic field. This corresponds to an approximately 0.28 m³ or 10 ft³ total volume around the inside of the ring. The magnetic field is made uniform by manipulating many magnetic ‘knobs’ built into the $g - 2$ storage ring, including the main magnet current, pole pieces, wedges, top hats, and thousands of small magnetic shims placed around the storage region. There is also an active feedback system which stabilizes the magnetic field over time. The shimming

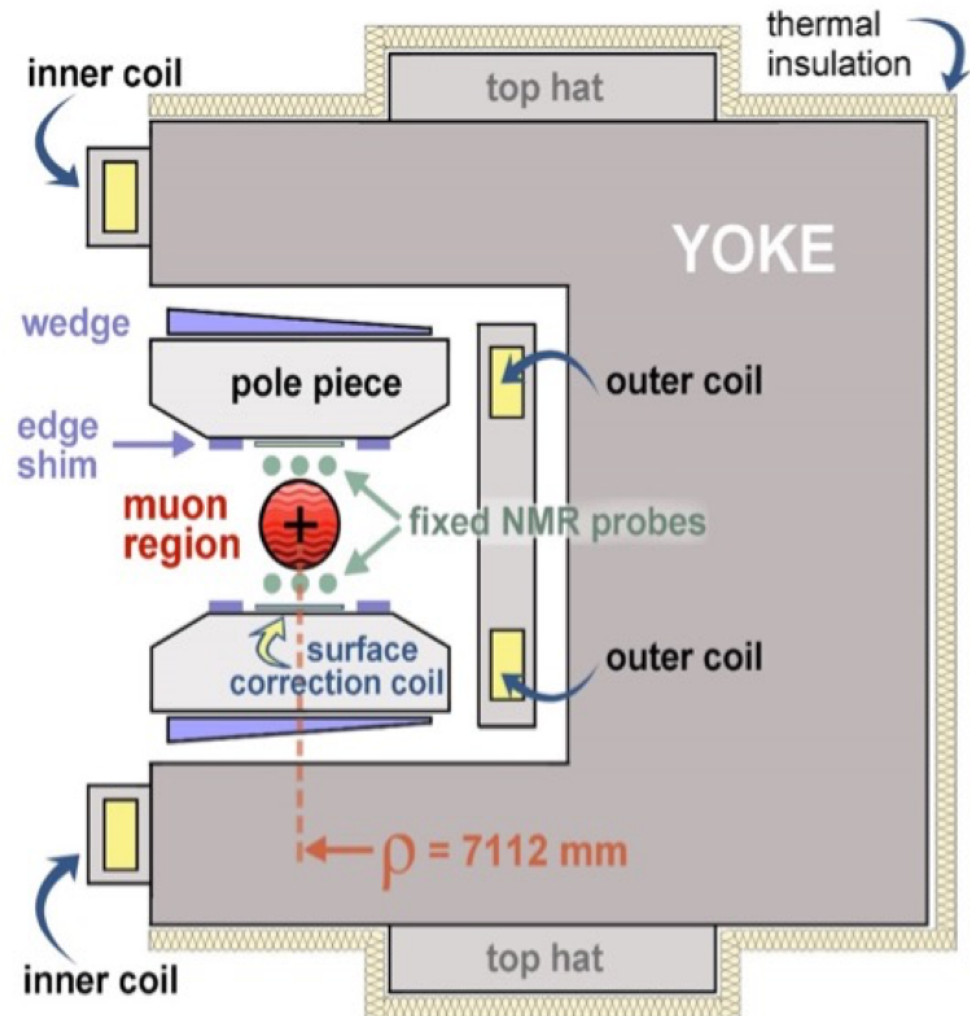
of the field to high precision, to an RMS (root mean square) of approximately 25 ppm, was a long process of fine tuning over the course of many months that was undertaken by many members of the field team.

Measuring the magnetic field comes down to measuring ω_p as shown in Equation [2.4]. This is because the magnetic field measurement is made using a pulsed nuclear magnetic resonance technique (NMR). NMR was chosen as it provides a field measurement precision on the order of 10 ppb with negligible statistical uncertainty [34]. NMR probes work by rotating the magnetization of a sample of protons in some fluid, typically water or petroleum jelly, and then measuring the relaxation time or free-induction decay (FID) signal of the proton spins. The magnetization of the protons will relax back to equilibrium with the external field as the spins of the protons precess at the Larmor frequency and interact with local magnetic field gradients or inhomogeneities. Pickup coils are located around the sample which both deliver the pulse to rotate the proton sample magnetization and measure the FID signal. An example of an FID signal is shown in Figure 2.6.

or viz.

~~Technically,~~ it is not solely ω_p that needs to be measured. What really matters is the average magnetic field that the muons see, ~~or~~ *namely* the time-averaged spatially-weighted magnetic field. The scheme devised to measure this is two-fold. First, the magnetic field in the storage region where the muons live is measured by a trolley which drives around the inside of the ring. This trolley holds 17 NMR probes and measures the field at approximately 6000 locations around the inside of the ring. Because ~~however~~ the trolley cannot be in the beam path when the muons are present in the ring, during data taking it is pulled out of the way and the field is instead measured by 378 fixed NMR probes located in the high magnetic field region, but just outside the storage region. The prescription is that the fixed probes measure the field at all times, the storage ring field is measured every few days by the trolley probes, and the two

on the outside of the vacuum chambers



g-2 Magnet in Cross Section

Figure 2-5: Cross-section of the $g - 2$ magnet. The muons live in the storage region. This is surrounded by many magnetic features of the magnet which allow for sub ppm level tuning of the magnetic field.

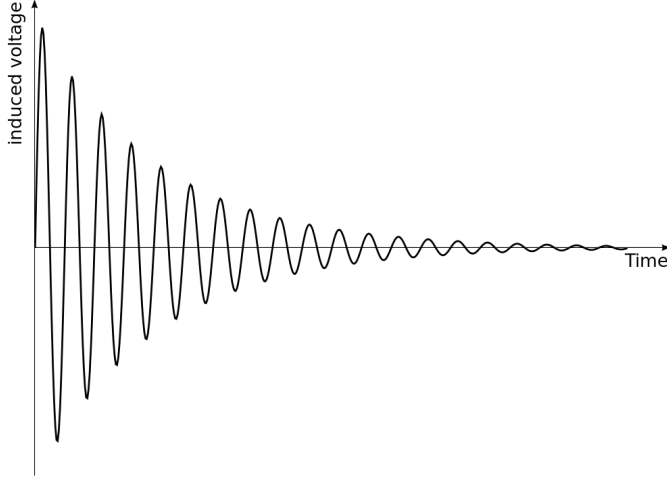


Figure 2.6: An example FID signal. The current picked up in the coils around the proton sample will oscillate as the spins precess around the main magnetic field, and decay as the spins return to alignment with the external field.

are interpolated. In this way the magnetic field can be mapped over time and over the space that the muons live in. A preliminary sample of the azimuthally-averaged magnetic field measured with trolley and fixed probes is shown in Figure 2.7.

Lastly, it is the free proton precession frequency in the field that is of interest, but the frequency that the probes measure will be different due to the molecular properties of the proton sample as well as the material properties of the probe itself. The frequency that the probes measure can be re-casted as

$$\omega_{p,\text{probe}} = \omega_{p,\text{free}}(1 - \sigma(\text{H}_2\text{O}, T) + \delta_b + \delta_p + \delta_s), \quad (2.16)$$

where $\sigma(\text{H}_2\text{O}, T)$ is the temperature dependent diamagnetic shielding of protons in a water molecule, and the δ 's come from corrections due to the bulk susceptibility of the water sample, paramagnetic impurities in the water sample, and the magnetic effects of the probe itself, respectively [34]. In order to correct for these effects two additional special probes are used, both of which live in a single section of the ring which has

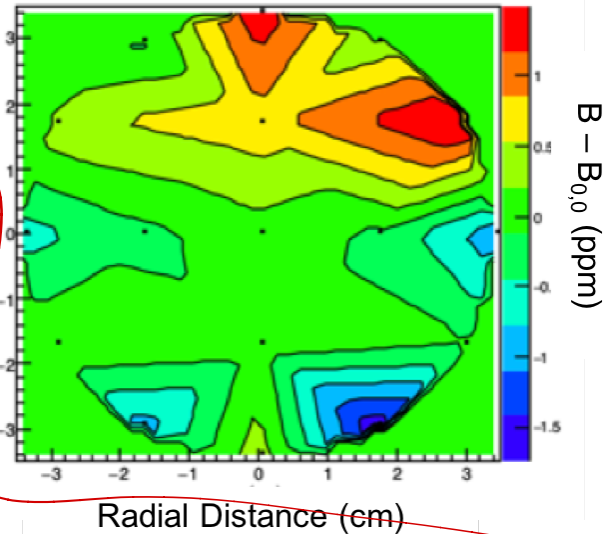


Figure 2·7: A sample of the azimuthally-averaged magnetic field within the storage region. The contours are normalized to the center value of the field. The scale of the field differences is approximately ± 1 ppm. The dots in the picture correspond to the location of the trolley probes. **Update this picture later on and find out what the time averaging is.**

*You should center fix
highly magnetic field
that is located*

been shimmed to extra uniformity. The first is a calibration probe which measures the free proton precession frequency at the center of the storage region corresponding to the placement of the central trolley probe. The calibration probe is made of materials in order to reduce the effects in Equation 2.16 and has been characterized in other test magnets. The second special probe is called the ‘plunging probe.’ This probe moves inside the vacuum chamber and drops into the storage region to measure the field at each of the 17 trolley probe locations, using a three dimensional motion system. By using these two probes, the calibration for the free proton precession frequency can be transmitted to each of the trolley probes, providing for the needed measurement inside the storage region of the magnetic field. This calibration procedure is estimated to take up about half of the target systematic uncertainty of 70 ppb ~~at~~ 35 ppb.

Other pieces of the systematic uncertainty include the absolute calibration of the

Magnetic Field Measurement Uncertainties	
Source of uncertainty	E989 Goal (ppb)
Absolute calibration of standard probe	35
Calibration of trolley probes	30
Trolley measurements	30
Fixed probe interpolation	30
Muon distribution weighted average	10
Time dependent external fields	5
Others	30
Quadrature sum	70

Table 2.1: Systematic errors in the magnetic field measurement. Unlisted sources of error include the measurement of higher field multipoles, trolley temperature and power supply voltage response effects, and eddy currents from the kicker, among others.

calibration probe, the trolley measurements, the interpolation to the fixed probes, the uncertainty relative to the muon distribution, and others such as time dependent external magnetic fields. See Table 2.1 When all is said and done, the measurement of the magnetic field is a complex and continuous process that is done in parallel to the measurement of ω_a throughout data taking.

2.3 Production of polarized muons

As explained previously, the number of high energy positrons detected depends on the direction of the muon spin at the time of decay. In order for this ~~detected quantity to mean anything, the ensemble of~~ measurement to work, the muon spins themselves need to be highly polarized. Using the same parity-violation and spin momentum conservation logic as expounded upon in muon decay, it is determined that pion decay produces muons that are 100% polarized in the pion rest frame, due to the pion having zero spin. The Feynman diagram for this decay is shown in Figure 2.1b. It's also important to note that pions decay to muons with over 99% branching ratio due to the parity violating nature of the weak

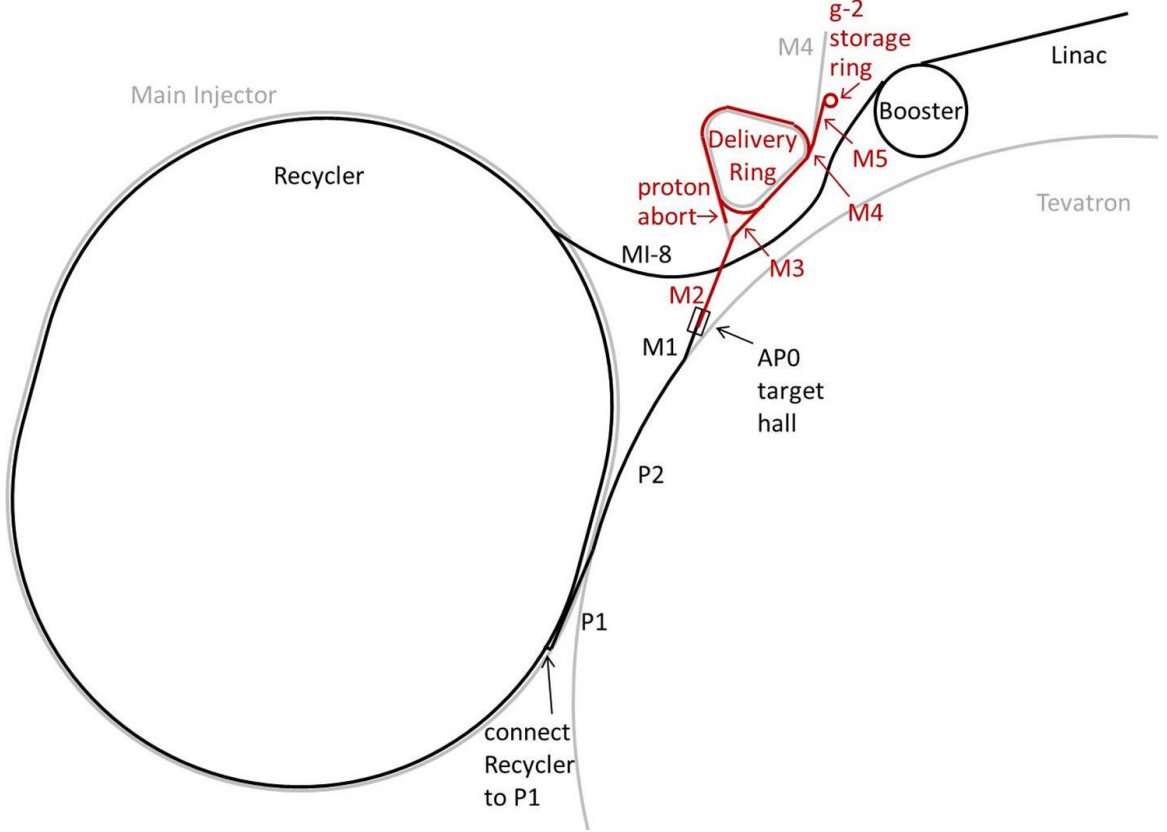


Figure 2.8: Plotted is the layout of accelerator beam-line components Fermilab uses to provide polarized muons to E989. Protons start in the Linac, traverse around the Booster and then Recycler, and are converted to pions at AP0. The pions are gathered and then decay away to muons in the Delivery Ring before being sent to the $g - 2$ storage ring. Figure taken from Reference [34].

interaction, and thus a preference for the heavier muon over the electron. These two facets of pion decay are used to construct polarized muon beams.

In order to measure $g - 2$ to high precision, a very large number of positrons need to be detected, and hence a large number of highly polarized muons injected into the storage ring. The BNL E821 experiment observed on the order of 10 billion positrons above threshold, and its final result was statistics limited. In order to reach the goal of 140 ppb, 20 times that number of statistics needs to be gathered. The only facility in the world that can produce such a high number of polarized muons is Fermilab.

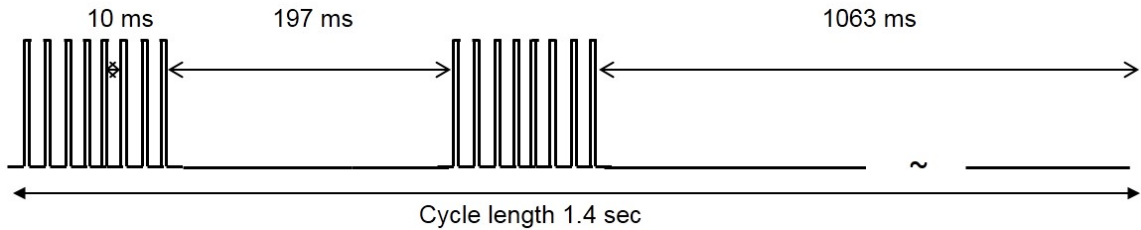


Figure 2.9: General timing structure of beam pulses sent to E989.

The Fermilab accelerator complex produces polarized muons for E989 in a number of stages. A map of the various relevant accelerator beam-line components is shown in Figure 2.8. Details of the full accelerator production of polarized muons can be found in Reference [35], and here will be given a summary of the process. First, protons are generated and accelerated in a linear accelerator. They are transported to a small circular ring called the “booster,” which accelerates them up to 8 GeV and batches them together. A single booster batch contains on the order of 4×10^{12} protons. The protons are then injected into a ring called “recycler,” which re-bunches them into four separate bunches of 1×10^{12} protons, each with a time width of approximately 120 ns. (This is less than the cyclotron period of the storage ring of 149 ns.) This rebunching process is done in order to reduce the level of pileup in the $g - 2$ detectors, see Section 3.2.1. For a single accelerator supercycle of 1.4 s, E989 receives four booster batches of particles corresponding to sixteen bunches at an average rate of 11.4 Hz, with the time separation between bunches greater than 10 ms. The timing structure is shown in Figure 2.9. The sets of eight bunches are sometimes referred to as pulses, and the gathered data is tagged by which bunch or pulse it originates from. Depending on the accelerator requirements of other experiments, this timing structure is modified appropriately though it is relatively constant.

Each bunch is selected one at a time and sent to a target hall, where the bunch is directed on to an Inconel target. This Inconel target is made up of a nickel and

I think it's 8 GeV/
Check this out

The production target

iron alloy optimized for producing a large number of pions with a small momentum spread, approximately $1 \times 10^{-5} \pi^+$ /POT with $|dp/p| < 2\%$ [35]. The resulting pions are focused just after production by a lithium lens. This lithium lens is a 1 cm radius and 15 cm long piece of lithium designed to carry high current which provides a radial focusing effect for particles passing lengthwise down the cylinder [36]. A pulsed magnet just after the lithium lens is then used to select pions at 3.115 GeV.

In a pion beam the highest and lowest energy decay muons are polarized. The pion beam and any residual protons or secondaries are injected into another ring called the “delivery ring”. By the time the pions have gotten to the delivery ring, most of them have decayed to muons. The delivery ring is used to both hold the beam until the remaining pions decay, which takes about four turns, and to select the polarized muons [35]. Forward emitted polarized muons are momentum selected at 3.094 GeV with $\Delta p/p = 2\%$. The remaining muons, protons, and other secondary particles are separated and Kicked into re-routed to a beam dump which reduces the contamination in the final polarized muon beam. This polarized muon beam is then sent to the $g - 2$ building where it passes through four magnetic quadrupole focusing magnets before being injected into the storage ring.

2.4 Injection of muons

The injection of the muon beam into the $g - 2$ storage ring is a specialized process. In order to measure the magnetic field to the precision described in Section 2.2, the $g - 2$ storage ring must be a single monolithic magnet with no end effects. This prohibits the usual design of separated magnetic elements through which the muons might be injected. Therefore we use a specialized magnet called the “Superconducting Inflector” magnet, or just inflector. This inflector is placed just after a bored out tunnel in the storage ring magnet, on the inside of the C shape. See Figure 2.10 for a

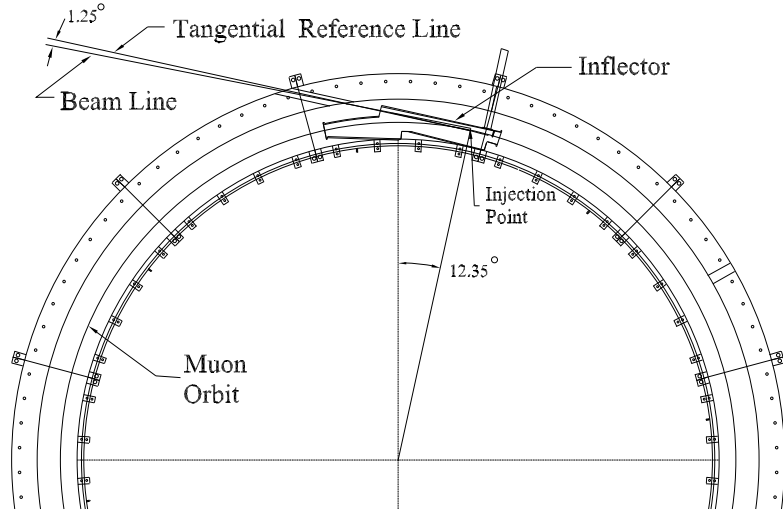
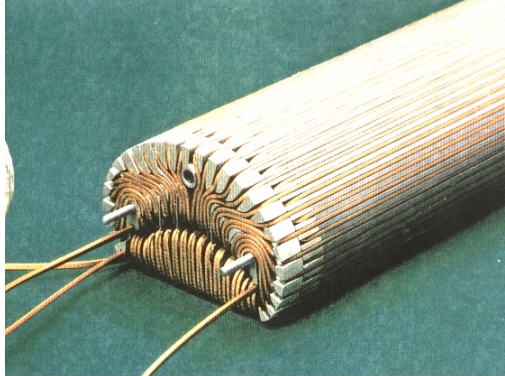
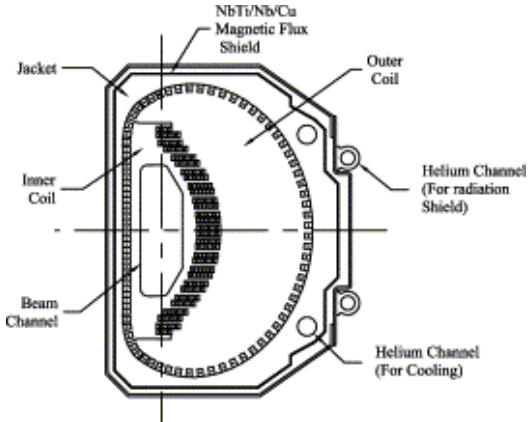


Figure 2·10: Shown is a plan view of the inflector and injection point into the storage ring [37].

view of the injection point. The inflector has a ~~very tight~~ 18 mm wide by 56 mm high aperture through which the muons must pass down its 1.7 m length. The inflector is made up of superconducting coils wrapped in a double cosine theta design around an aluminum mandrel [37]. See Figure 2·11. This design serves to contain the majority of the inflector magnet field, while eliminating the the storage ring field for the muons passing down its length, such that they are not lost due to ~~motion~~ ^{deflection} induced by said field. The inflector is contained within a superconducting shield which traps the fringe field of the inflector such that the storage ring magnet field is unaffected. As shown in Figure 2·11, both sides of the inflector are closed such that an appreciable fraction of muons are lost due to multiple scattering before being injected into the ring. Approximately 2% of injected muons are stored with $\Delta p/p = 0.1\%$ centered around 3.094 GeV. A new inflector magnet is being designed with open ends in order to increase the muon flux for future runs of $g - 2$ [34].



(a) End view of the inflector.



(b) Cross section view of the inflector.

Figure 2·11: The inflector magnet (left) and a cross section view of the inflector windings and associated shield (right) [37].

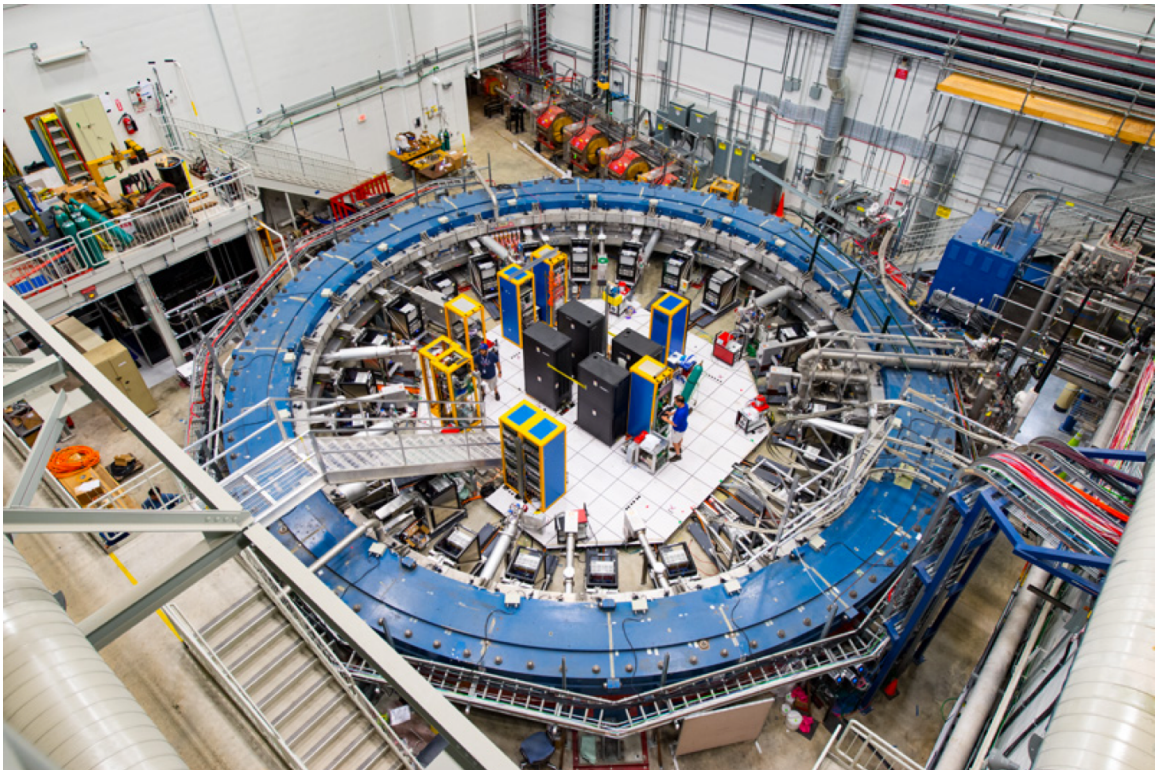


Figure 2·12: Shown is a picture of the $g - 2$ experiment. The blue ~~painted~~ storage ring can be seen to surround a variety of detectors and electronics. Muons come in at the top of the picture through a ~~series~~ series of magnetic quadrupoles from the accelerator and are injected into the ring, where they orbit in a clockwise direction. There are ~~some~~ ^{Two} people located inside the ring which gives a sense of scale to the picture.

give

2.5 Storage of muons

The E989 experiment and storage ring are shown in Figure 2-12. Approximately 10,000 muons are stored in the $g - 2$ ring at a time, corresponding to a single fill. The 3.094 GeV muons will decay with a lifetime of approximately 64.4 μs . Once the muons have been injected into the ring, they will begin orbitting clockwise around the ring. By necessity, the inflector must be out of the stored muon beam path, otherwise a large fraction of the muons would be lost upon the return to the injection point as the muons would strike the inflector. Therefore the muon beam must be manipulated to move to switch the orbit path from the injection orbit onto the central orbit around the center of the storage ring. Once the muon beam is centered, it must also be focused vertically, otherwise all of the muons would be lost due to the vertical motion of the helical path of the muons. To perform the former, a magnetic “kicker” is used to shift the orbits of the muons. To perform the latter, a series of electrostatic quadrupoles focus the beam vertically.

2.5.1 Kicker

The kicker is made up of three separate pulsed magnets located 90° from the exit of the inflector, where the inflector orbit crosses the central orbit. The placement of the kickers is shown in Figure 2-13. It's important to note that the kicker must be operated within the magnetic field of the ring, and must therefore contain no magnetic elements in the hardware itself which would perturb the uniform magnetic field. For this reason the kicker is made up of thin aluminum plates which carry the current used to create the kicking magnetic field. Due to the bunched nature of the muon beam and the short cyclotron period of 149 ns, ideally the kicker moves all stored muons onto the central orbit and then turns off quickly such that by the time the muons orbit back around to the kicker there is no residual kick to the beam. Any

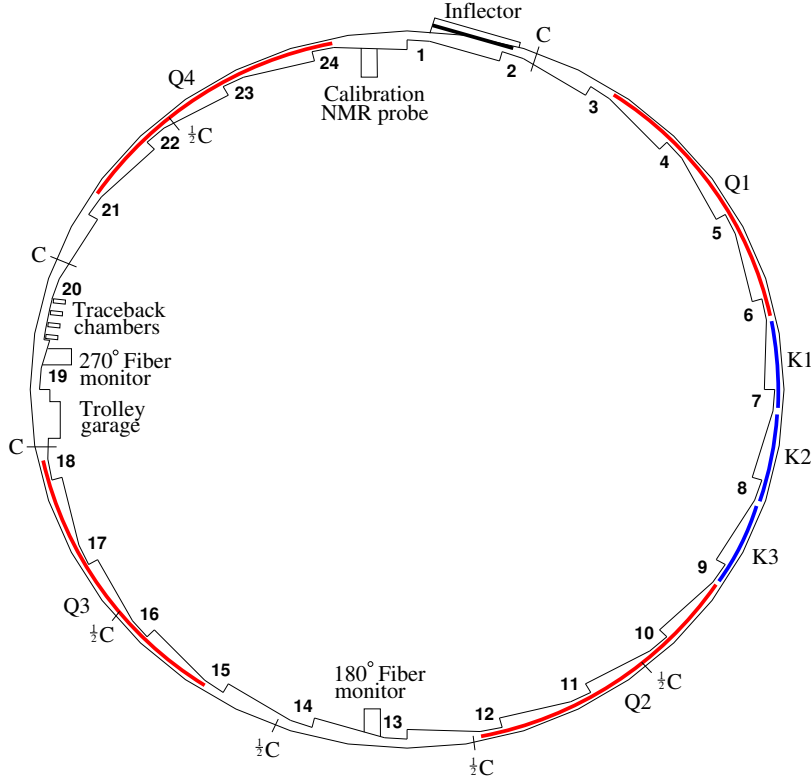


Figure 2·13: A map of the vacuum chambers in E989. K1-K3 show the locations of the kicker magnets, while Q1-Q4 show the locations of the electrostatic quadrupoles. Also shown is the location of the inflector, the two fiber monitors, and one of the tracker stations.

residual eddy currents must die away quickly enough that the magnetic field seen by the stored muons is unperturbed. The kick to the beam is approximately 10 mrad using a vertical pulsed field of around 300 Gauss over three 1.27 m long magnets and with a pulse length of about 120 ns.

2.5.2 Electrostatic quadrupoles

There are four electrostatic quadrupoles (quads) located around the ring as shown in Figure 2·13, which focus the beam vertically and defocus the beam horizontally. (The magnetic field of the ring serves to restore the beam radially in combination with the electric field.) Just as in the case of the kickers, the quads must be operated in the

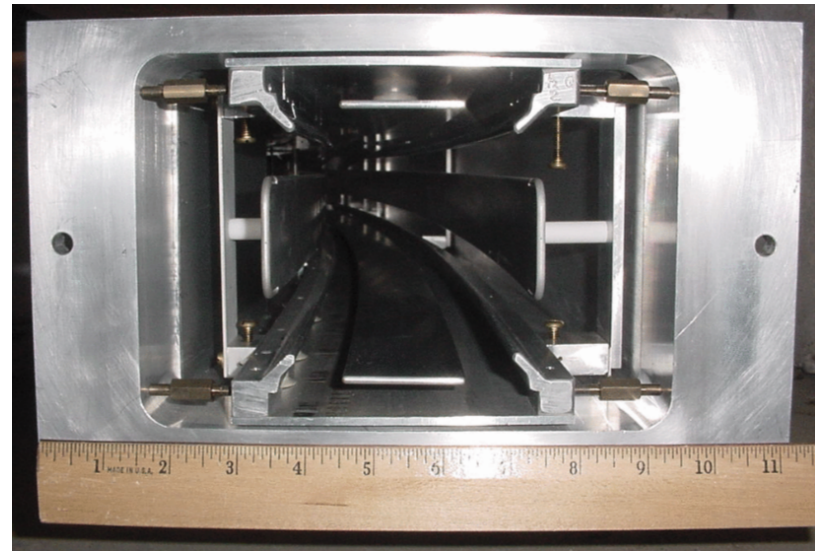


Figure 2·14: Electrostatic quadrupoles installed into a vacuum chamber [38]. There are four plates mounted to the chamber through insulator standoffs. Also shown are the rails that the magnetic field trolley rides on around the inside of the ring, and between the quad and kicker plates. The distance between opposing quad plates is 10 cm.

vacuum. E989 uses electrostatic focusing elements instead of magnetic ones in order to avoid magnetic field gradients which would limit the precision of the magnetic field measurement. Four quads were chosen in order to ~~maximize the symmetry of the beam motion around the ring~~ ^{with fourfold symmetry of the quadrupole}. The quads occupy 43% of the ring circumference, leaving space for other elements around the ring. Each quad is made up of two segments, a short segment of 13° and a long segment of 26°. The quads are made out of as little material as possible in order to reduce multiple scattering of decay positrons passing through them. A picture of the quads installed into one of the vacuum chambers is shown in Figure 2·14. A simulation of the equipotential lines of the quads is shown in Figure 2·15. The original design of the quads is detailed in Reference [38].

Lastly, some of the stored muons will be lost during data taking that will affect the measurement of the precession frequency ω_a . In order to reduce the number of

I would do a global change quad \rightarrow quadrupole

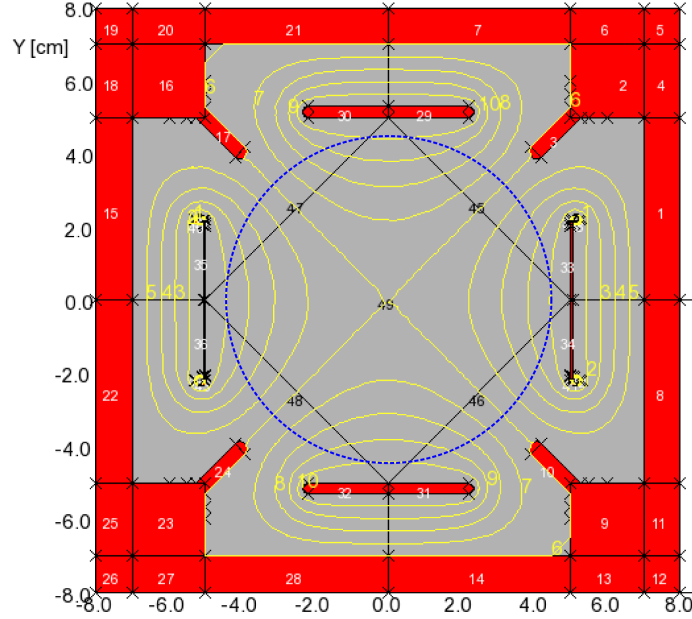


Figure 2.15: An OPERA model of the quads and their equipotential contours. The top and bottom plates sit at positive voltage while the left and right plates are at negative voltage. The muon storage region is shown by the blue circle. Picture from Reference [34].

lost muons over the course of a fill, a procedure called “scraping” is used to remove those muons sitting at the edge of the storage region that will likely be lost at later times. This scraping procedure involves powering the quad voltages in an asymmetric way such that the beam is pushed to the outside of the storage region, where the edges of the beam will intersect copper collimators. Muons which hit the collimators will lose energy and be lost as they spiral out of the ring. The scraping procedure is performed early in the fill and ends at something²⁰ μ s. Note that despite this scraping procedure, some stored muons are still lost anyways. The effects on the measurement of ω_a due to this are explored in Section 5.3.

talk with Jason Cr.
& get the correct
time constants

2.6 Muon beam dynamics

Muons injected into the storage ring will occupy a region in phase space corresponding to a width of momenta and positions. Individual muons will undergo simple harmonic motion or betatron oscillations within the storage ring, in both the vertical and horizontal directions. The strength of the electrostatic focusing in relation to the magnetic field strength can be characterized by the field index

$$n = \frac{\kappa R_0}{\beta B_0}, \quad (2.17)$$

where κ is the electric quadrupole gradient, B_0 is the magnetic field strength, R_0 is the central storage ring radius, and β is the relativistic velocity of the muon beam. The horizontal and vertical equations of motion, including the effects of the discrete quadrupoles, are given by

$$x = x_e + A_x(s) \cos(\nu_x \frac{s}{R_0} + \phi_x), \quad (2.18)$$

$$y = A_y(s) \cos(\nu_y \frac{s}{R_0} + \phi_y), \quad (2.19)$$

where x_e is the radial equilibrium orbit of the beam relative to R_0 , $A_x(s)$ and $A_y(s)$ are the amplitudes of the motions containing the effects of the discreteness of the quads, and s is the arc length of the trajectory. Here ν_x and ν_y are the so-called horizontal and vertical “tunes” of the beam motion, which are ratios of the betatron frequencies to the cyclotron frequency. They can be related to the field index n by

$$\begin{aligned} \nu_x &= f_{x_{BO}}/f_c = \sqrt{1-n}, \\ \nu_y &= f_{y_{BO}}/f_c = \sqrt{n}, \end{aligned} \quad (2.20)$$

where f_c is the cyclotron frequency. Technically n is the average field index around the ring, where this approximation is justified due to the four-fold symmetry of the

Muon Beam Frequencies				
Name	Symbol	Expression	Frequency (MHz)	Period
$g - 2$	f_a	$a_\mu Be/2\pi mc$	0.23	4.365 μ s
cyclotron	f_c	$v/\pi R_0$	6.71	149 ns
horizontal betatron	$f_{x_{BO}}$	$\sqrt{1-n}f_c$	6.34	158 ns
vertical betatron	$f_{y_{BO}}$	$\sqrt{n}f_c$	2.21	452 ns
coherent betatron	f_{CBO}	$f_c - f_{x_{BO}}$	0.37	2.703 μ s
vertical waist	f_{VW}	$f_c - 2f_{y_{BO}}$	2.31	433 ns

Table 2.2: Frequencies seen in the $g - 2$ experiment due to beam motion. Parameter values are from a subset of Run 1 corresponding to an n value of 0.108 or a quad voltage of 18.3 kV.

discrete quadrupoles and the fact that the betatron oscillations have periods much greater than the length of the quads. A table of the important frequencies in E989 is shown in Table 2.2. Lastly, the maximum angular acceptance of the ring can be determined from the betatron oscillations and the field index as

$$\begin{aligned}\psi_{x_{max}} &= \frac{x_{max}\sqrt{1-n}}{R_0}, \\ \psi_{y_{max}} &= \frac{y_{max}\sqrt{n}}{R_0},\end{aligned}\tag{2.21}$$

where x_{max} and y_{max} are both equal to the radius of the storage ring aperture at 45 mm.

As the muon beam goes around the ring, the muons will experience local field gradients and inhomogeneities. The tunes are thus chosen to avoid resonances where muons might be lost from having passed through such perturbations too many times. The muons within the ring should then sample the entire azimuth equally and remain stored. The general resonance condition is [39]

$$a\nu_x + b\nu_y = c,\tag{2.22}$$

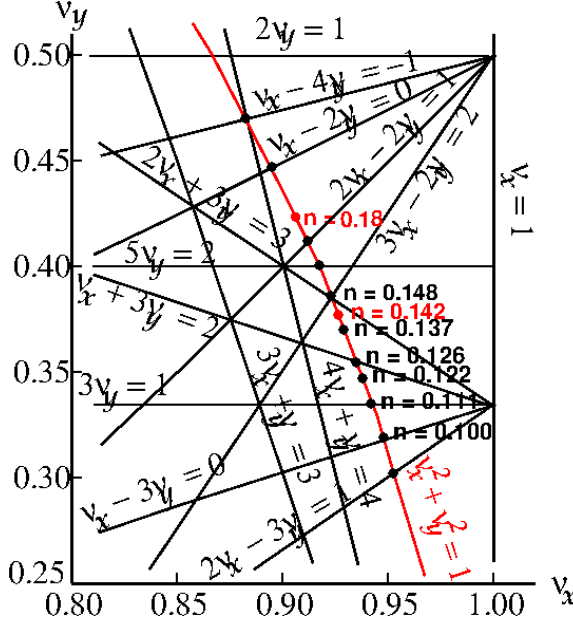


Figure 2.16: The tune plane, with the $v_x^2 + v_y^2 = 1$ constraint in red. The chosen value of n lies on this circle. The original design goals for E989 were the n values as shown by the red points, but due to hardware issues smaller n values of 0.108 and 0.120 were chosen as described in Section 2.8.

where a , b , and c are integers. We know from Equation 2.20 that

$$\text{this is (only) approximately correct unless } v_x^2 + v_y^2 = 1, \quad (2.23)$$

since the quadrupole field only

which constrains the available n values that can be chosen. Figure 2.16 shows the space relative to the tunes for which a chosen value of n will lie on a resonance.

2.6.1 Coherent betatron oscillation

With each individual muon undergoing betatron oscillations, the muon beam as a whole will oscillate. The beam can be described as having a width and a mean dependent on the initial phase space parameters determined by injection and kicker effects. This overall distribution of the beam will oscillate coherently every betatron wavelength, thus moving around the ring at some frequency. Individual detectors

Why does the CBO appear in the
Cyclotron spectrum? 38
The acceptance depends on the radial
distance.

around the ring measure the beam in discrete pieces based on their individual acceptances, where these acceptances depend on the radial and vertical characteristics of the beam. Because the betatron frequencies are smaller than the cyclotron frequency, there is an aliasing effect such that the betatron motion of the beam is instead observed as an apparent slow-moving oscillation. We call the measurable signal of this coherent radial motion coherent betatron oscillation (CBO). See Figure 2.17 for a pictorial view of this phenomena. The frequency of the CBO is just the beat frequency between the cyclotron frequency and the horizontal betatron frequency

$$f_{CBO} = f_c - f_{x_{BO}}. \quad (2.24)$$

You mean vertical but that must be much smaller

~~There is also a horizontal CBO effect, but the rate of oscillation is fast enough that~~
the effect tends to average out. What can be seen in the data however is the vertical width of the beam, to which the detectors are sensitive. Though the principles are the same, we call this effect the vertical waist (VW),

$$f_{VW} = f_c - 2f_{y_{BO}}, \quad (2.25)$$

isn't it is an imaging of the vertical aperture of the inflector.
where the term waist is used a description of the vertical width when its at its minimum. Both of these frequencies are included in Table 2.2. For an individual detector the CBO has a specific phase, which goes from 0 to 2π around the ring. When adding all of the detector signals together, the CBO effect tends to cancel out. However, due to acceptance differences between the different detectors, the CBO effect is still observable in the data. When fitting the data to extract ω_a , these effects need to be included as will be discussed later.

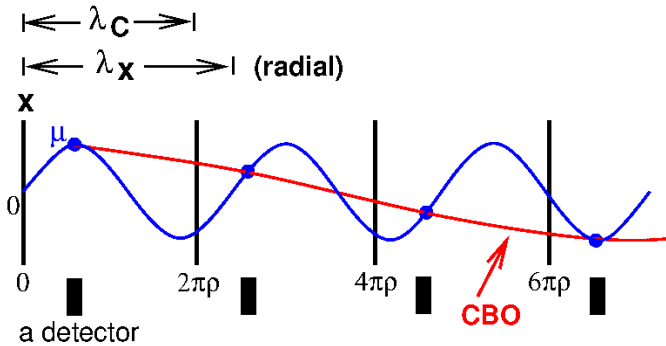


Figure 2.17: Marked by the black vertical lines are integer steps in the circumference of the ring, corresponding to the cyclotron wavelength λ_c . The blue line shows the motion of the beam due to the betatron oscillations λ_x . Since $\lambda_x < \lambda_c$, there is an aliasing effect in the observed signal, which is identified by the red line. The beam is thus seen as appearing to move back and forth with a slow oscillation, and this is what we call CBO.

To a single detector the beam appears to move slowly

2.6.2 Beam debunching

As described above, the muon beam is injected into the ring with a time spread of 120 ns and a range of momenta. At early times the beam will occupy a portion of the ring less than the whole since the cyclotron period is 149 ns. Therefore early in the fill the detectors located at discrete points around the ring will measure counts from the beam where there will be a fast oscillation in the signal due to this cyclotron period. As time increases throughout the fill, the momentum distribution of the muons will cause the beam to spread out within the storage ring until the entire azimuth is filled. Since almost all muons are at the same momentum, it turns out that the ~~slower moving~~ ^{tail of} muons at smaller radii catch up to the ~~faster moving~~ muons at the outer radii after many turns around the ring. By 30 μ s the muon beam has gone around the ring two hundred times. As the beam fills the storage ring, the cyclotron frequency in the ~~decreases as~~ ^{it appears} ~~decreases and~~ ^{it appears} the beam ~~is seen to~~ ^{it appears} debunch. This phenomena is referred to as the “fast rotation.” See Figure 2.18 for how ~~this looks~~ ^{it appears} in the data. When dealing with the data and attempting to extract ω_a , the typical procedure is to both bin

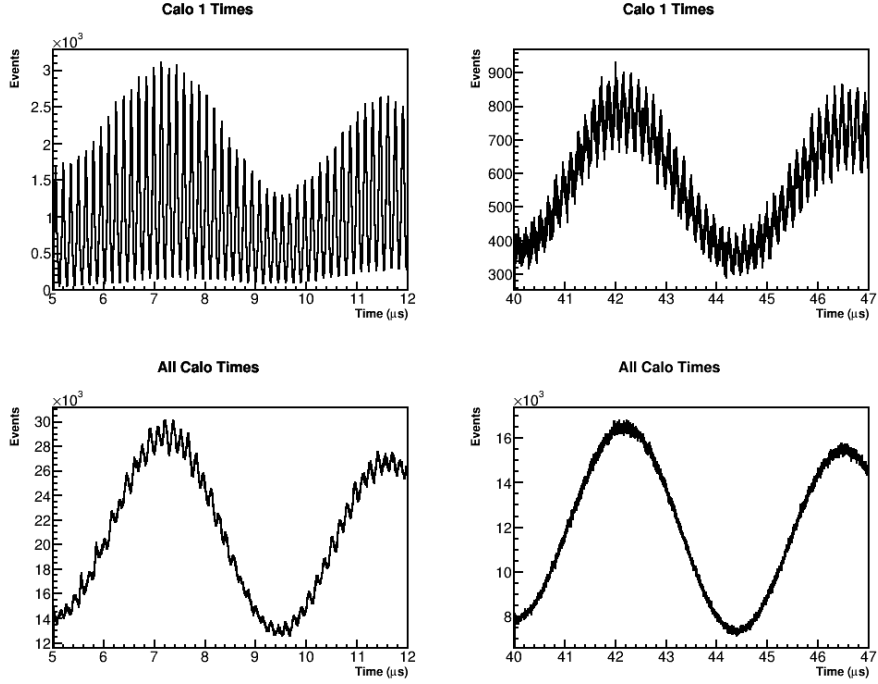


Figure 2.18: The fast rotation signal can be seen in the data as an oscillation with a period of 149 ns, corresponding to the fast oscillations in these plots. In individual calorimeters at early times the fast rotation signal is seen to be very large, as shown on the top left. As time passes and the beam debunches, the amplitude of the fast rotation signal diminishes as shown on the top right. When adding all calorimeters together, the signal reduces as shown in the bottom two plots. In all cases the slow oscillation is the $g - 2$ frequency.

out the fast rotation in periods of the cyclotron frequency, and to randomize each hit time by $\pm T_c/2$ where T_c is the cyclotron period. In this way the fast rotation is removed entirely and the five parameter function described in Equation 2.13 remains satisfactory, barring other effects.

2.7 Corrections to ω_a

Equation 2.3 is an idealized version of the spin difference frequency. Including practical experimental concerns, there are two corrections that must be applied to ω_a .

2.7.1 Electric field correction

In the presence of an electric field, the spin difference frequency is altered to

$$\vec{\omega}_a = -\frac{q}{m} [a\vec{B} - \left(a - \frac{1}{\gamma^2 - 1}\right)(\vec{\beta} \times \vec{E})], \quad (2.26)$$

where now there is an extra term dependent on the electric field strength and the momentum of the particles. This is necessary to include since we use electrostatic quadrupoles for vertical focusing as described above. The second term cancels to first order for a specific momentum or value of γ . This "magic momentum" can be understood as the momentum at which a relativistic particle moving through an electric field has its spin exactly follow its momentum. This magic momentum is 3.094 GeV for muons, hence the momentum value of the injected muons. This value has driven many of the design constraints of the $g - 2$ experiment, including the size of the storage ring, choice of the magnetic field magnitude, and so on.

you can do a better job

Not all muons will have the magic momentum however as described in the Section 2.3, and therefore a correction to the measured ω_a frequency needs to be applied. Approximating the storage ring as having an electric field applied over the whole azimuth of the ring, the spin difference frequency for muons with momentum $p \neq p_m$ (where p_m is the magic momentum) becomes

$$\omega'_a = \omega_a \left[1 - \beta \frac{E_r}{cB_y} \left(1 - \frac{1}{a\beta^2\gamma^2} \right) \right]. \quad (2.27)$$

B + E motion field a magnetic field

Here the motion of the beam is assumed purely azimuthal. This additional term is the electric field correction that then serves to lower the measured ω_a frequency. Using the relation $p = \beta\gamma m = (p_m + \Delta p)$, after a little bit of simplification the electric field correction can be written as

$$C_E = \frac{\Delta\omega_a}{\omega_a} = -2 \frac{\beta E_r}{cB_y} \frac{\Delta p}{p_m}. \quad (2.28)$$

The last fraction can be related to the field index described in Equation 2.17 by

$$\frac{\Delta p}{p_m} = (1 - n) \frac{\Delta R}{R_0} = (1 - n) \frac{x_e}{R_0}, \quad (2.29)$$

are central radius R_0

since we know that the magic momentum muons live at the center of the storage ring radius R_0 . In this equation $x_e = \Delta R$ is the equilibrium radius of the beam relative to the central storage radius. Noting that the radial electric field strength is

$$E = \kappa x = \frac{n\beta c B_y}{R_0} x, \quad (2.30)$$

and assuming that it is perfectly radial, the electric field correction can be reduced to

$$C_E = -2n(1 - n)\beta^2 \frac{x x_e}{R_0^2}. \quad (2.31)$$

Taking the time average of the beam motion, where x is simply equal to x_e , the correction becomes

$$C_E = -2n(1 - n)\beta^2 \frac{\langle x_e^2 \rangle}{R_0^2}. \quad (2.32)$$

This electric field correction can be determined through analysis which relates the beam momentum to the equilibrium radius. (Should I expand on that somehow here?)

The assumptions made here are sufficient for the $g - 2$ measurement [something].

2.7.2 Pitch correction

Fast notation $\rightarrow \langle x_e \rangle$

Particles injected into the $g - 2$ storage ring will have some motion component that is vertical, or parallel to the magnetic field vector (hence the need for vertically focusing electrostatic quadrupoles). This will reduce the magnetic field seen by the muons in their rest frame slightly. Including this motion into the spin difference frequency

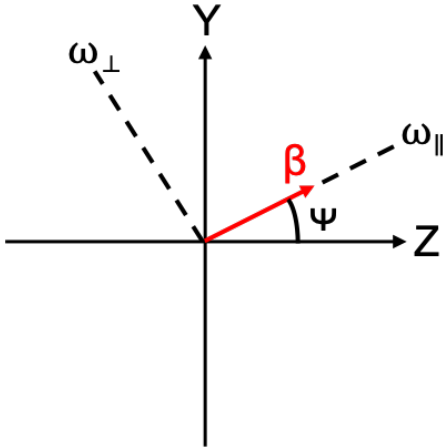


Figure 2.19: Beam motion β relative to the vertical and azimuthal axes Y and Z respectively. ψ is the pitch angle of the beam, and the dashed lines represent the parallel and perpendicular motions of the beam.

(along with the electric field correction described previously), ω_a becomes

$$\vec{\omega}_a = -\frac{q}{m} [a\vec{B} - a\left(\frac{\gamma}{\gamma+1}\right)(\vec{\beta} \cdot \vec{B})\vec{B} - \left(a - \frac{1}{\gamma^2-1}\right)(\vec{\beta} \times \vec{E})], \quad (2.33)$$

the second comes from
 where now there is an extra term in the middle dependent on the vertical betatron motion of the beam. Similar to the electric field case, this term can be neglected to first order as the muon momentum is nearly all perpendicular to the field, but a correction again needs to be applied to ω_a to account for this effect.

Since the muons in the storage ring will be oscillating vertically as they are focused by the quads, their momentum vectors will be pitching up and down relative to the azimuthal motion. This pitch angle will oscillate as

$$\psi = \psi_0 \cos(\omega_y t), \quad (2.34)$$

where ψ_0 is the amplitude of the oscillation and ω_y is the vertical betatron frequency. Shown in Figure 2.19 is an exaggerated example of the beam motion relative to the vertical and azimuthal axes. Assuming that the field is purely vertical, $\vec{B} = B_y \hat{y}$ and

that the beam motion is in the vertical-azimuthal plane,

$$\vec{\beta} = \beta_y \hat{y} + \beta_z \hat{z} = \beta \cos(\psi) \hat{y} + \beta \sin(\psi) \hat{z}, \quad (2.35)$$

then ω_a becomes

$$\vec{\omega}_a = -\frac{q}{m} [a B_y \hat{y} - a \left(\frac{\gamma}{\gamma+1} \right) \beta_y B_y (\beta \cos(\psi) \hat{y} + \beta \sin(\psi) \hat{z})], \quad (2.36)$$

where in this case the electric field part has been ignored. Using the small angle approximation such that $\cos(\psi) \approx 1$ and $\sin(\psi) \approx \psi$, $\vec{\omega}_a$ can be separated into its vertical and azimuthal components

$$\omega_{ay} = \omega_a \left[1 - \left(\frac{\gamma-1}{\gamma} \right) \psi^2 \right], \quad (2.37)$$

$$\omega_{az} = -\omega_a \left(\frac{\gamma-1}{\gamma} \right) \psi. \quad (2.38)$$

Looking at Figure 2.19 again, it can be seen that the spin difference frequency can be resolved into its parallel and perpendicular components ω_{\parallel} and ω_{\perp} respectively. As the pitch angle of the beam motion oscillates about the azimuthal axes at a frequency much greater than the $g - 2$ frequency, it can be seen that the parallel component averages to 0 over time. (Haven't given a number for the vertical betatron frequency yet.) We then only care about the perpendicular oscillation of the beam, which can be determined with a simple rotation matrix such that

$$\omega_a \approx \omega_{\perp} = \omega_{ay} \cos(\psi) - \omega_{az} \sin(\psi) \approx \omega_a \left[1 - \frac{\psi^2}{2} \right], \quad (2.39)$$

where in the last approximation the small angle approximation was used once again, but this time with $\cos(\psi) \approx 1 - \psi^2/2$. The pitch correction then is the additional term which serves to lower the measured spin difference frequency. Taking the time

note that the 4-fold ^{quad} symmetry also
 says that $\sqrt{\frac{\beta_{y\max}}{\beta_{y\min}}} = 1.03$ 45
 average,

$$C_P = \frac{\Delta\omega_a}{\omega_a} = -\frac{\langle y^2 \rangle}{2} = -\frac{\langle \psi_0^2 \rangle}{4}, \quad (2.40)$$

See E821 Quad paper.

where Equation 2.34 was used in the last equality. The pitch angle of the beam cannot be measured directly, however we know from Equation 2.21 that the angle of the beam can be related to the vertical distribution of the beam, such that

$$C_P = -\frac{n}{4} \frac{\langle y^2 \rangle}{R_0^2} \neq 3 \quad (2.41)$$

where Once again n is the field index, R_0 is the radius of the ring at the center of the storage region, and $\langle y^2 \rangle$ is the vertical width of the beam. The first two are known and the last can be measured experimentally. (For this last equation make sure that what I write here gels with what I'll put in other sections, which haven't been done yet.) While this derivation was an approximation assuming continuous quads around the ring, it suffices for the level of precision necessary for the $g - 2$ experiment [something].

2.8 Run 1 in E989

by the frackers

Run 1 for E989 was conducted in the first half of 2018. Production data ~~was~~ gathered from March 22nd through June 29th. The number of injected muons per fill was $\mathcal{O}(4,000)$. Because of accelerator, experimental, and practical concerns production data taking was interrupted at various dates. Due to hardware issues both kicker and quad settings were originally lowered from their technical design values. Various voltage set points for both systems were identified and used in separate periods of the data taking, depending on the stabilities of the systems. The distinct designated datasets gathered by E989 and their associated parameters are shown in Table 2.3. Due to the lower kicker voltages, the muon beam was stored on a radius several mm offset from the central orbit of the storage ring, as shown in Figure 4.23. The

chosen quad n values were 0.108 and 0.120, corresponding to quad voltages of 18.3 and 20.4 kV respectively [40]. The associated betatron wavelengths are 1.06 and 3.04 times the circumference of the storage ring respectively. During Run 1 it was also discovered that some of the quad resistors were damaged, leading to longer RC time constants such that the quad voltages had not reached storage nominal at the beginning of the designated analysis portion of the data, and were still changing over the course of a fill. See Figure 2.20. The muon beam was therefore seen to move as a function of time in-fill. See Section 4.4 for a summary of the muon beam characteristics for Run 1. As described in various sections in this chapter and in Section 4.4, these muon beam characteristics fold into the measurement of $g - 2$ in a variety of ways, for which work is still on-going.

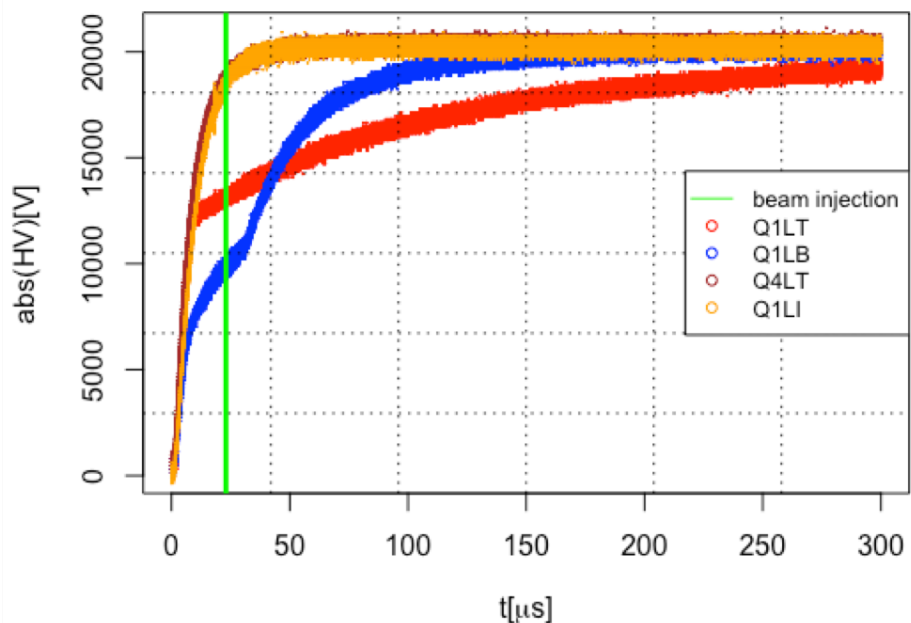


Figure 2.20: Traces for the high voltages as a function of time on some of the quad plates. The different plates are identified in the legend, where for instance Q1LT stands for the top long plate of quad 1. The beam is injected at the green line and the scraping procedure occurs until the quad voltages relax to their design values, in this case 20.4 kV. As shown some of the high voltage traces do not relax in a smooth and fast exponential manner, due to damaged quad resistors. The traces in orange and brown are for good quad resistors, while the traces in red and blue show the results from damaged quad resistors. Plot courtesy of

Since R is very large
 $\tau_{RC} = RC$
 is large
 explain the RC time constant
 at the beginning of the
 decay part on p 24

Run 1 Datasets					
Name	Number $e^+ > E_{\text{Th}}$	n	Value	Quad Voltage (kV)	Kicker Voltage Range (kV)
60H	9.3×10^8	0.108	18.3		128 – 132
HighKick		0.120	20.4		136 – 138
9d	2.2×10^9	0.120	20.4		128 – 132
LowKick		0.120	20.4		123 – 127
SuperLowKick		0.108	18.3		117 – 119
Endgame		0.108	18.3		122 – 127
Total Positrons Above Threshold					

Table 2.3: The different designated datasets acquired during Run 1 of E989 and their associated parameters [41]. Update the number of positrons column once all of the datasets have been opened and energy thresholds chosen. Potentially also add further columns of interest or split into multiple tables.